Selection of Emission Wavelength of Lasing via a Hybrid Microcavity

Hong Yang,[1] Hailang Dai,[1,*] Qiheng Wei,[1] Hongrui Shan,[1] Zhuangqi Cao,[1] and Xianfeng Chen[1,2,3,4,†]

[1] *The State Key Laboratory on Fiber Optic Local Area Communication Networks and Advanced Optical Communication Systems, Department of Physics and Astronomy, Shanghai Jiao Tong University, Shanghai 200240, China*

[2] *Shanghai Research Center for Quantum Science, Shanghai 201315, China*

[3] *Jinan Institute of Quantum Technology, Jinan 250101, China*

[4] *Collaborative Innovation Center of Light Manipulations and Applications, Shandong Normal University, Jinan 250358, China*

(Received 8 April 2021; revised 30 June 2021; accepted 27 August 2021; published 8 September 2021)

In the applications of optical communication and light-matter interaction manipulation, the capability of on-demand lasing output with programmable and continuous wavelength tunability over a broad spectral range under low threshold is key functionality. However, the ability to control multiwavelength lasing characteristics within a small mode volume with high reconfigurability remains challenging. The number of dyes and the emission wavelengths of existing materials always restrict the color gamut. In this Letter, we introduce a selection of emission wavelength laser by injecting Rhodamine 6G solution mixed with Au nanoparticles in the metal-cladded slab-capillary hybrid microcavity. A mechanism for tuning laser emission wavelengths is designed by manipulating the diameter of Au nanoparticles in Rhodamine 6G solution. Precision control of distinctive lasing wavelengths and a narrower peak are achieved, along with a stable lasing beam output from both ends of the capillary due to coherent superposition. Our findings offer possibilities for realizing a micro selection of emission wavelength laser from a single overall structure.

DOI: 10.1103/PhysRevApplied.16.034015

I. INTRODUCTION

A tunable laser with a selection of wavelength via the capability of a single chip has been a subject of great interest in recent years, with the realization of a selection of emission wavelength tunable laser as the ultimate goal. In fact, obtaining the desired emission wavelength, maintaining stability for a long time, and having an ultranarrow linewidth is particularly useful for laser lighting, optimal wavelength laser imaging and display [1,2], and biological and chemical sensing, as well as on-chip wavelength-division multiplexing [3]. Meanwhile, the tunable laser has extensive application prospects in the fields of communication [4], biology and pharmaceuticals [5], and especially in future optical communication systems [6]. In practice, the tunable fiber laser and the semiconductor tunable laser are two main types of tunable laser. The tunable fiber laser can be directly coupled to the transmission fiber, and has the advantages of a large tuning range through adjusting the cavity length, low transmission loss, and high output power. However, the unstable output wavelength of the lasing beam and slow speed of adjustment hinder application of the fiber laser. As for the semiconductor tunable laser, there are several common types. The distributed feedback (DFB) laser with different fixed wavelengths can be manufactured as a multiwavelength array integrated laser [7,8]. It has the advantages of good monochromaticity, narrow linewidth, and high side-mode suppression ratio. However, this type of laser suffers from the dissipation of output lasing power, because it will increase along with the increasing number of wavelengths due to nonuniform transmission and distribution. Meanwhile, the thermal tuning method adopted by DFB lasers results in slower response speed, higher power consumption, lower yield, and low repeatability. Another type of electro-optically tuned distributed Bragg reflector (DBR) technique [9], is used to produce a tunable laser, which achieves a freely tunable wavelength within a certain range. Moreover, the tuning time resolution can be reduced to nanoseconds. The complexity of calibration and high cost of production of the DBR tunable laser hinder its promotion and application. Generally, the external cavity wavelength tunable laser achieves wavelength tuning by changing the angle of the external cavity diffraction grating using a microelectromechanical system (MEMS) [10]. The MEMS has the advantages of narrow linewidth, large tuning range, and stability [11]. However,

*hailangdai@sjtu.edu.cn
†xfchen@sjtu.edu.cn

its restrictions include the large size, difficulty of alignment of light path, and unavailability of fast tuning due to the long time taken for mechanical adjustment of the external cavity filter. The vertical-cavity surface-emitting laser [12] with a relatively small volume and ease of access for integration has been studied in recent years. It outputs a weak optical power with a relatively high current drive due to a large internal resistance. A larger optical power output can be produced by the MEMS structure. However, this increases the volume and cost of the laser, and the accuracy and speed of wavelength tuning cannot be guaranteed [13].

A selection of emission wavelength laser is developed using a hybrid microcavity composed of a symmetrical metal-cladded slab waveguide (SMSW) and a hollow-core capillary to overcome limitations such as randomness, high threshold, etc. A mechanism for tuning laser emission wavelengths is designed by manipulating the diameter of Au nanoparticles in Rhodamine 6G (R6G) solution. Precision control of distinctive lasing wavelengths and a narrower peak are achieved. The SMSW structure promotes the localized surface plasmon resonance of the Au nanoparticles, making the lasing threshold under continuous-wave pumping become 5.7 μW/mm^2. Figures 1(a) and 1(b) show the schematic structure and electromagnetic field distribution for the slab-capillary microcavity. The effective index of the waveguideN_{eff} is between 0 and 1 due to the symmetrical metal cladding, and as a result, light can still be trapped in the waveguide layer without leakage after the liquid with low refractive index is injected into the waveguide layer, so that the interaction between light and matter can be fully achieved in the waveguide layer. Therefore, the R6G solution mixed with Au nanoparticles of different diameters emits lasers of different wavelengths due to the resonant wavelengths of the Au nanoparticles being related to their size.

We add nanoparticles of uniform size to the dye, and emit lasing of a specific wavelength through the overall effect of plasmon resonance, which is related to the diameter of the nanoparticle. The dye can absorb heat, and its thermal effect is very weak, thus this selection of emission wavelength laser holds promise for more stable lasing under similar conditions. In comparison, the thermal expansion effect, light leakage, fiber materials, and other factors cause instability of fiber lasers. As for the adjustment speed of the adjustable laser, the fiber laser adjusts the output lasing by temperature or current, while this selection of emission wavelength laser excites lasing of different wavelengths directly through multiple channels with different sizes of Au nanoparticles [14]. Furthermore,

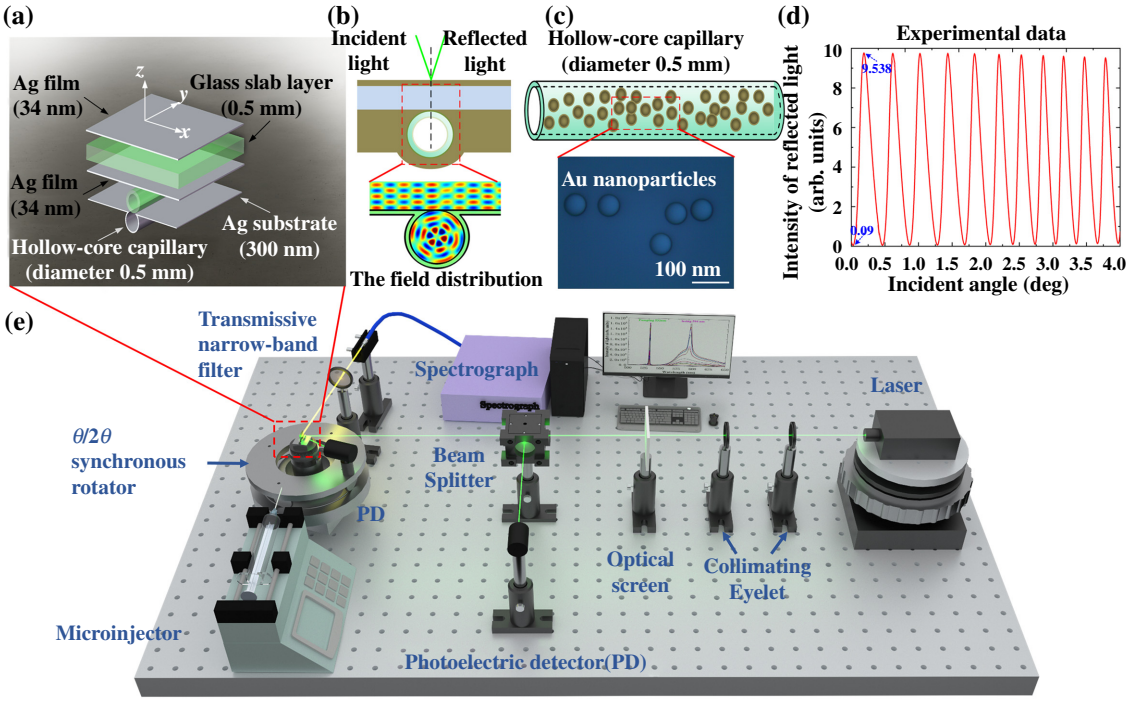

FIG. 1. Structural characterization and experimental system in the metal-cladded slab-capillary hybrid microcavity. (a) Schematic diagram of the hybrid microcavity. (b) Electromagnetic field distribution for the slab-capillary microcavity using COMSOL software. (c) Injecting R6G solution with Au nanoparticles by a microinjector into the hollow-core capillary [25]. (d) Reflectance spectra of the modes for the slab-capillary waveguide versus the incident angle. (e) Experimental system and setup, the chip is fixed on the $\theta/2\theta$ synchronous rotator and rotated by a personal computer(PC).

this selection of emission wavelength laser has the advantages of easy preparation, availability for integration, and small size.

II. STRUCTURAL CHARACTERIZATION AND EXPERIMENTAL SYSTEM

As shown in Fig. 1(a), the waveguide structure of the microcavity chip is 10 mm long and 10 mm wide, including a 0.5-mm-thick glass slab as the base of the chip. The upper and lower surfaces of the glass slab are parallel (less than 4 in.). The glass slab and a capillary with an outer diameter of 0.5 mm are used as the guide layers. The upper silver film (about 34 nm thick) can couple the pump light into the waveguide. Another 300-nm-thick silver film is utilized as a substrate layer. In such a waveguide, the thin metal coupling layer and the small effective refractive index enable the direct coupling of light from the free space into the guiding layer without any additional coupler, such as a grating or high-index prism [15–20]. At small incident angles, the standing optical field oscillates rapidly through the linear cavity between the metallic coupling layer and substrate [see Fig. 1(b)], resulting in various properties, such as strong field enhancement, high sensitivity, high quality factor, and polarization independence [14,21–24].

Capillary oscillations are governed by surface tension and distinguished from acoustic oscillations. These oscillations play a major role in microstructure coalescence and are also an important phenomenon in interface theories. Moreover, the metal cladding of the capillary helps couple its interior modes with the SMSW transmission modes, and traps these modes into the hollow core of the capillary. Therefore, a high-density resonant electromagnetic field is formed in the hollow core as the field has been limited by two-dimensional constraints [see Fig. 1(b)]. Practically, the design allows most of the ultrahigh order modes (UOMs) of the SMSW to excite the capillary eigenmodes enhancing the mode spacing. For the chip with a capillary, the UOMs are coupled into the capillary and the field distribution inside the capillary. We use the COMSOL software to fit the field distribution. In our previous research, we achieved white and tunable lasing through controlled injection of different dye solutions into the capillaries [14], and we have obtained more interesting results based on this structure recently. In this study, R6G and Au nanoparticles with a diameter of 50 nm are injected into the hollow-core capillary [see the microscope image in Fig. 1(c)]. The incident light is coupled into the waveguide layer when the incident angle reaches a specific coupling angle obtained from the mode eigenvalue equation of the SMSW. The SMSW structure is introduced to enhance the excitation of the resonance modes in the gain medium. This waveguide chip includes a millimeter-thick resonance cavity filled with an active medium, which permits the hosting of thousands of guided modes, that is, UOMs. At small incident angles, continuous-wave 532 nm incident light (Coherent Inc Verdi, USA) is coupled into the hybrid microcavity and the light field oscillates rapidly in the cavity between the metal coupling layer and the substrate in Fig. 1(b), resulting in the lasing emission through scattering in a series of concentric rings. We measure the spectral reflectance of the microcavity chip by changing the angle of the incident light, and obtain a coupling efficiency of 99% from the air to the capillary experimentally, owing to the free space coupled technology, as shown in Fig. 1(d).

III. RESULTS AND DISCUSSION

We select R6G as a gain medium [see Fig. 2(a)] because of the broad linear width of its fluorescence spectrum around the wavelength of 570 nm. Furthermore, the resonant wavelengths of 10–100-nm-sized Au nanospheres accord with the fluorescence spectrum in the R6G solution. In the experimental system, the R6G solution mixed with Au nanospheres with a diameter of 50 nm are injected into the hollow-core capillary using a syringe pump (PHD 2000, Harvard Apparatus), while a 532 nm pump light with a coupling efficiency of 99% (continuous-wave diode-pumped solid-state laser, maximum power 20 mW, spot size 1.0 mm^2) is applied to the capillary, as shown in Fig. 2(b). Eventually, we detect a lasing beam with a wavelength of approximately 594 nm, and obtain laser spectroscopy using a spectrograph (Andor Shamrock 500i, Oxford Instruments) and an image using a CCD (Zyla 5.5 Scmos, Oxford Instruments) at the end of the capillary, as shown in Figs. 2(c) and 2(e). This CCD observes a bright beam of light emitted from the end face, while broadband fluorescence is absorbed and leaked into the metal-cladded layer of the capillary without a resonance wavelength. The intensity of the lasing beam increases with pumping energy, and the peak laser intensity becomes more obvious [see Fig. 2(d)].

As shown in Fig. 3, the lasing peak appears as the power of the pump light reaches 5.7 $\mu W/mm^2$ (the intensity of incident light is 5.7 μW and the size of incident light spot is 1.0 mm^2), and it gradually increases with the intensity of input pumping [see Fig. 3(a)]. The lower threshold is mainly due to UOMs, high density of power, and localized surface plasmon resonance (LSPR) of Au nanospheres [14,25]. Figure 3(b) shows the relationship between the pump light input into the capillary and the output laser light intensity. The pump light with three different powers of P1–P3 makes the lasing peak gradually increase and the center wavelength is fixed at approximately 593 nm, as shown in Fig. 3(c).

In the same experimental system, we employ Au nanospheres with the different diameters of 40 and 60 nm (all within the range of the R6G fluorescence spectrum) in the R6G solution, and then inject into the hollow-core capillary. We discover that the emission wavelength of

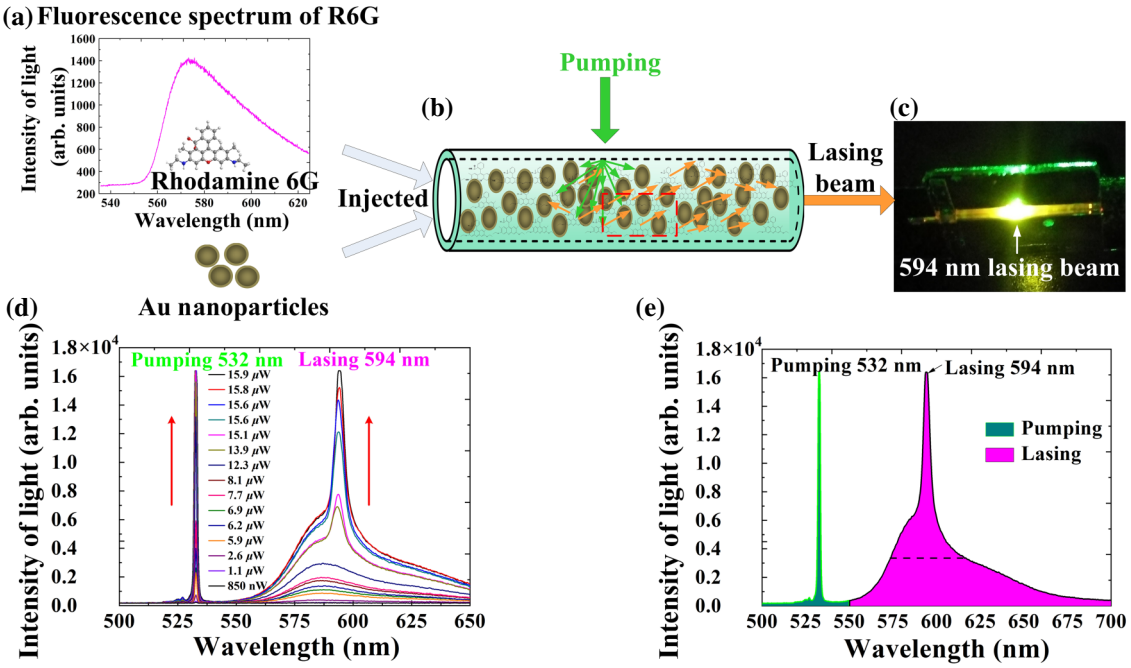

FIG. 2. Laser emission in the capillary hybrid microcavity. (a) Fluorescence spectrum of R6G. (b) Injection of Au nanoparticles and R6G into the capillary under the action of pump light can catch the lasing beam. (c) Approximately 594 nm laser beam after passing through the transmissive narrow-band filter. (d) The laser intensity at approximately 594 nm varies with the pump light at 532 nm. (e) The spectrum of the pumping and laser beam using the spectrograph.

lasing changes accordingly with the manipulation of the diameter of the Au nanospheres. The red and black lines depict the fluorescence spectrum of R6G and the laser spectrum at different intensities of pumping. The output spectrum corresponds to the stronger pump light power, which is described by the black line. With Au nanoparticles with a diameter of 40 nm, the lasing beam with a wavelength of 560 nm appears on both the red and black lines [see Fig. 4(a)]. Figure 4(c) shows that the Au nanoparticles with a diameter of 60 nm have a laser of around

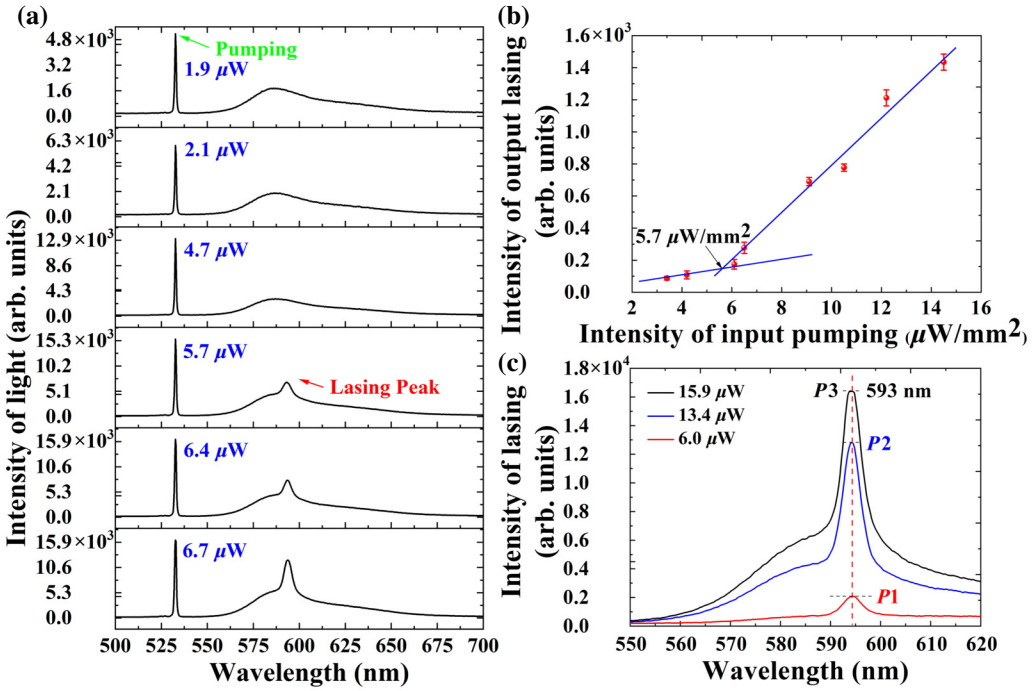

FIG. 3. The relationship between input pumping and output lasing. (a) The threshold of lasing. (b) The relationship between intensity of input pumping and output lasing. (c) The intensity of lasing corresponding to the three intensities of the input pumping.

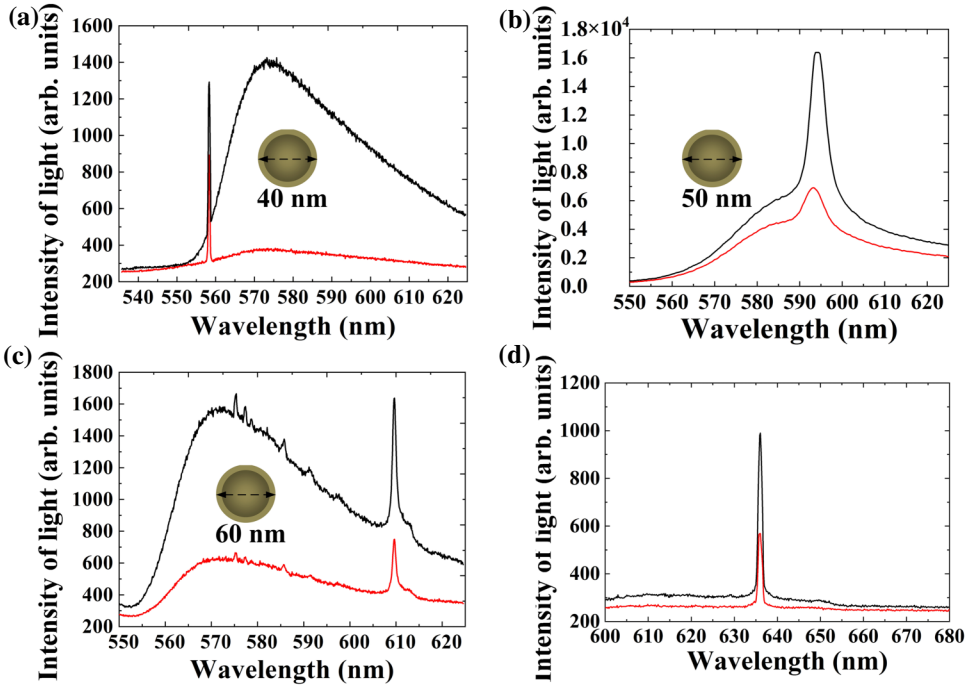

FIG. 4. Comparison of laser beams after injecting Au nanoparticles with different diameters. (a)–(c) The intensity of light from the capillary mixed with Au nanoparticles of 40, 50, and 60 nm. The black line corresponds to a stronger pump light power (∼10 μW) while the red line corresponds to a pump light power of approximately 5 μW. (d) The intensity of light from the capillary without Au nanoparticles.

610 nm, and the laser peak always increases with the power of the pump light. The laser wavelength is about 636 nm when R6G without nanoparticles is injected into the hollow-core capillary [see Fig. 4(d)]. Comparing the linewidths of the lasing beams with nanoparticle diameters of 40, 50, and 60 nm, the linewidth for 50 nm is broader than that of the others because the resonant wavelength for 50 nm is near the center of fluorescence spectrum of R6G. Figure 4(d) shows that the lasing beam emits at single wavelength without Au nanoparticles, the wavelength of lasing is closely related to the size of the cavity and the diameter of the capillary [14,25]. This selection of emission wavelength laser is a dye laser. The spontaneous emission ability of the dye solution in the SMSW is enhanced, which leads to a broader linewidth. On the other hand, the chosen-diameter Au nanoparticles injected into the R6G are not exactly a single diameter and the existence of these deviations causes the linewidth of the lasing to become broader. This work verifies that the diameter of the Au nanospheres is closely related to the laser wavelength, meaning that the laser wavelength increases with the diameter of the Au nanospheres, which demonstrates this selection of emission wavelength laser.

IV. THEORY AND SIMULATION OF STRUCTURE

To elucidate the underlying mechanism of laser wavelength selecting behavior, we examine the theory and simulation of the structure based on the finite-difference time-domain algorithm [26] to calculate the resonance optical properties of several diameter Au nanospheres in R6G. When the incident light frequency is consistent with the free-electron oscillation frequency on the surface of metal nanoparticles, the Au nanoparticle produces the near-field distribution of LSPR, and the wavelength of the incident light that excites free-electron oscillation is the resonance wavelength. The high density of power is symmetrically distributed on the surface of nanoparticle. Meanwhile, the LSPRs of single Au nanoparticles will not interfere with each other [25].

According to the Mie scattering theory of electromagnetic fields, the resonant wavelength of Au nanoparticles is closely related to the size of the nanoparticles. Therefore, we simulate and calculate the scattering efficiency, extinction efficiency, and absorption efficiency of Au nanospheres with a diameter of 40, 50, and 60 nm in R6G [see Figs. 5(a)–5(c)]. The extinction efficiency of Au nanospheres with a diameter of 40 nm reaches a peak when the incident light wavelength is approximately 586.3 nm, as shown in Fig. 5(a). Therefore, the resonance wavelength of the 40-nm-diameter Au nanospheres is approximately 586.3 nm. In a similar way, the resonance wavelengths of Au nanospheres with a diameter of 50 and 60 nm are approximately 596.4 and 604.8 nm [see Figs. 5(b) and 5(c)]. As shown in Fig. 5(d), the diameter of the Au nanoparticles is set from 40 to 120 nm at 10 nm intervals. The resonance wavelength and resonance extinction efficiency gradually increase with the diameter of the Au nanoparticles. According to the results, the extinction efficiency and resonant wavelength of Au nanoparticles are directly proportional to the diameter of the Au nanoparticles. The relevant factors can realize the regulation of the LSPR of Au nanoparticles [27–29]. Compared with simulation results, the resonance wavelengths of Au

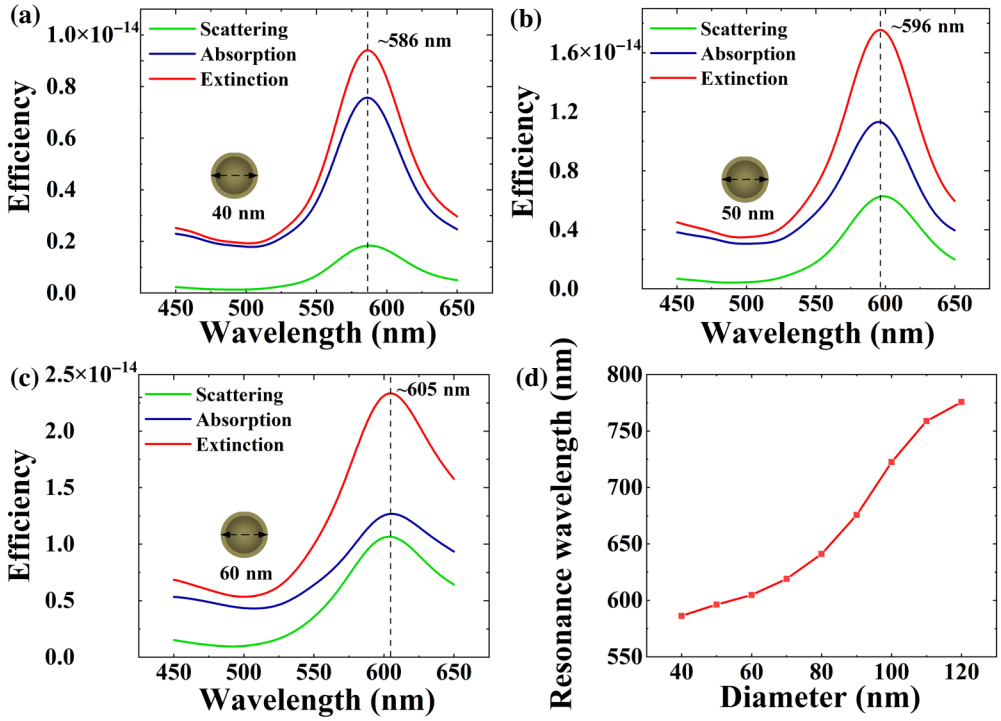

FIG. 5. Theory and simulation of the structure. (a)–(c) The scattering efficiency, extinction efficiency, and absorption efficiency of Au nanospheres with a diameter of 40, 50, and 60 nm in R6G. (d) The resonance wavelength of Au nanospheres varies with diameter in R6G.

nanospheres with a diameter of 40, 50, and 60 nm in R6G solution match the laser wavelengths [see Figs. 4(a)–4(c)]. The resonant wavelengths of 50 and 60 nm are near the center of the fluorescence spectrum of R6G, which make them more consistent with the Mie scattering theory. The actual resonance wavelength for a diameter of 40 nm leads to a deviation from the fitting of the Mie scattering theory of electromagnetic field. These wavelengths are contained within the fluorescence spectrum of R6G, causing the LSPR of Au nanospheres with diameters of 40, 50, and 60 nm. Consequently, a significant selection of lasing wavelength can be observed for certain diameter Au nanoparticles in dye solution. Moreover, the resonance light is enhanced by LSPR and amplified by coherent addition along the transmission direction. The previously mentioned phenomena agree well with our experimental results and assumptions.

V. CONCLUSION

In summary, we develop a tuning wavelength laser that can generate an on-demand laser and directly output the lasing beam from the microcavity. Most importantly, an approach to tuning the laser wavelength is proposed by adjusting Au nanospheres with different diameters in a hybrid microcavity at room temperature. The findings clearly show that the wavelength of the lasing beam can be selected by injecting dye solutions mixed with different metal nanoparticles into the metal-cladded capillary of the microcavity. Our work simplifies the process of creating an integrated laser structure with a controllable wavelength, and achieves precise wavelength regulation, which is an important step towards the realization of a potentially miniature, integrated structure of tunable laser devices. It also promotes the development of a miniaturized multiwavelength laser source, providing possibilities for programmable light sources and biomedical devices with devisable lasing emission in the future.

ACKNOWLEDGMENTS

Funding for this work is from the National Key R&D Program of China (Grant No. 2018YFA0306301); the National Natural Science Foundation of China (NSFC) (Grants No. 11734011 and No. 11764020); the China Postdoctoral Science Foundation (Grant No. 2020M681275); and the Foundation for Shanghai Municipal Science and Technology Major Project (Grant No. 2019SHZDZX01-ZX06).

[1] M. W. Berns, Partial cell irradiation with a tunable organic dye laser, Nature **240**, 483 (1972).
[2] H. Farrokhi, T. M. Rohith, J. Boonruangkan, S. Han, H. Kim, S. W. Kim, and Y. J. Kim, High-brightness laser imaging with tunable speckle reduction enabled by electroactive micro-optic diffusers, Sci. Rep. **7**, 15318 (2017).
[3] Z. F. Zhang, X. D. Qiao, B. Midya, K. Liu, J. B. Sun, T. W. Wu, W. J. Liu, R. Agarwal, J. M. Jornet, S. Longhi, N. M. Litchinitser, and L. Feng, Tunable topological charge vortex microlaser, Science **368**, 760 (2020).

[4] H. Al-Taiy, N. Wenzel, S. Preußler, J. Klinger, and T. Schneider, Ultra-narrow linewidth, stable and tunable laser source for optical communication systems and spectroscopy, Opt. Lett. **39**, 5826 (2014).
[5] V. S. Letokhov, Laser biology and medicine, Nature **316**, 325 (1985).
[6] P. Miao, Z. F. Zhang, J. B. Sun, W. Walasik, S. Longhi, N. M. Litchinitser, and L. Feng, Orbital angular momentum microlaser, Science **353**, 464 (2016).
[7] P. Rauter and F. Capasso, Multi-wavelength quantum cascade laser arrays, Laser Photonics Rev **9**, 452 (2015).
[8] O. S. M. Sadeghi, W. Li, X. Li, and W.-P. Huang, Purely loss-coupled distributed feedback lasers based on electromagnetically induced absorption in active photonic band gaps, Phys. Rev. A **75**, 063829 (2007).
[9] G. Gilardi, R. Asquini, A. d'Alessandro, and G. Assanto, Widely tunable electro-optic distributed Bragg reflector in liquid crystal waveguide, Opt. Express **18**, 11524 (2010).
[10] B. Mroziewicz, External cavity wavelength tunable semiconductor lasers - a review, Opto-Electron. Rev. **16**, 347 (2008).
[11] X. M. Zhang, A. Q. Liu, D. Y. Tang, and C. Lu, Discrete wavelength tunable laser using microelectromechanical systems technology, Appl. Phys. Lett. **84**, 329 (2004).
[12] H. Soda, K.-i. Iga, C. Kitahara, and Y. Suematsu, Gainasp/InP surface emitting injection lasers, Jpn. J. Appl. Phys. **18**, 2329 (1979).
[13] C. J. Chang-Hasnain, Tunable vcsel, IEEE J. Sel. Top. Quant. **6**, 978 (2000).
[14] H. L. Dai, C. Yin, Z. Y. Xiao, Z. Q. Cao, and X. F. Chen, White Beam Lasing from a Hybrid Microcavity with Slab-Capillary Mode Coupling, Phys. Rev. Appl. **11**, 064055 (2019).
[15] H. L. Dai, B. Jiang, C. Yin, Z. Q. Cao, and X. F. Chen, Ultralow-threshold continuous-wave lasing assisted by a metallic optofluidic cavity exploiting continuous pump, Opt. Lett. **43**, 847 (2018).
[16] H. F. Lu, Z. Q. Cao, H. G. Li, Q. S. Shen, and X. X. Deng, Polarization-independent and tunable comb filter based on a free-space coupling technique, Opt. Lett. **31**, 386 (2006).
[17] G. A. Wurtz, R. Pollard, W. Hendren, G. P. Wiederrecht, D. J. Gosztola, V. A. Podolskiy, and A. V. Zayats, Designed ultrafast optical nonlinearity in a plasmonic nanorod metamaterial enhanced by nonlocality, Nat. Nanotechnol. **6**, 107 (2011).
[18] N. Hermosa, A. M. Nugrowati, A. Aiello, and J. P. Woerdman, Spin Hall effect of light in metallic reflection, Opt. Lett. **36**, 3200 (2011).
[19] L. Chen, Z. Q. Cao, F. Ou, H. G. Li, Q. S. Shen, and H. C. Qiao, Observation of large positive and negative lateral shifts of a reflected beam from symmetrical metal-cladding waveguides, Opt. Lett. **32**, 1432 (2007).
[20] X. B. Yin, Z. L. Ye, J. Rho, Y. Wang, and X. Zhang, Photonic spin Hall effect at metasurfaces, Science **339**, 1405 (2013).
[21] H. L. Dai, C. Yin, X. N. Ye, B. Jiang, M. W. Ran, Z. Q. Cao, and X. F. Chen, A possible pathogenetic factor of sickle-cell disease based on fluorescent analysis via an optofluidic resonator, Sci. Rep. **7**, 3174 (2017).
[22] D. Kumar and V. Singh, Theoretical modeling of a nonlinear asymmetric metal-clad planar waveguide based sensors, Optik **122**, 1872 (2011).
[23] K. T. Kim, H. W. Kwon, J. W. Song, S. Lee, W. G. Jung, and S. W. Kang, Polarizing properties of optical coupler composed of single mode side-polished fiber and multimode metal-clad planar waveguide, Opt. Commun. **180**, 37 (2000).
[24] Y. Wang, Z. Q. Cao, T. Y. Yu, H. G. Li, and Q. S. Shen, Enhancement of the superprism effect based on the strong dispersion effect of ultrahigh-order modes, Opt. Lett. **33**, 1276 (2008).
[25] See Supplemental Material at http://link.aps.org/supplemental/10.1103/PhysRevApplied.16.034015 for the structural characterization, the theory of structure, and the simulation results of structure, which includes Refs. [14–20].
[26] K. Yee, Numerical solution of initial boundary value problems involving Maxwell's equations in isotropic media, IEEE Trans. Antennas Propag. **14**, 302 (1966).
[27] S. Ma, D. J. Yang, S. J. Ding, J. Liu, W. Wang, Z. Y. Wu, X. D. Liu, L. Zhou, and Q. Q. Wang, Tunable Size Dependence of Quantum Plasmon of Charged Gold Nanoparticle, Phys. Rev. Lett. **126**, 173902 (2021).
[28] J. Parsons, E. Hendry, C. P. Burrows, B. Auguié, J. R. Sambles, and W. L. Barnes, Localized surface-plasmon resonances in periodic nondiffracting metallic nanoparticle and nanohole arrays, Phys. Rev. B **79**, 073412 (2009).
[29] E. Petryayeva and U. J. Krull, Localized surface plasmon resonance: Nanostructures, bioassays and biosensing—A review, Anal. Chim. Acta. **706**, 8 (2011).